structure of surfaces and interfaces, for example, the value of z and the distributed width for z.

From the reciprocity theorem, the calculation of fluorescent x-ray intensity Y from coordinate z on the take-off angle θ_t is identical with that of incident x-ray field at coordinate z on the glancing angle θ_t. Thus, when atoms act as fluorescent x-ray sources with a distribution N, the yield Y should be

$$Y(\theta_t) = \int I(\theta_g, \lambda_p, z)\, N(z, \sigma)\, I(\theta_t, \lambda_f, z)\, dz \quad (1)$$

where $I(\theta_g, \lambda_p, z)$ is the primary x-ray intensity, which is affected by the total reflection beams for the incident wavelength λ_p at coordinate z. The distribution $N(z, \sigma)$ reaches a maximum at $z = z_0$ and is assumed to obey a Gaussian distribution with standard deviation σ (see Fig. 2). The intensity $I(\theta_t, \lambda_f, z)$ for fluorescent x-ray wavelength λ_f results from interference between the direct and totally reflected fluorescent emissions at coordinate z.

We obtained z_0 and the width 2σ for χ^2 minimization fit for $Y(\theta_t)$. The theoretical FXI pattern is in close agreement with the experimental one (Fig. 4). The values of the refractive indices of the gold substrate and of the LB film were obtained from the separate fitting of the x-ray reflectivities at the corresponding four wavelengths.

The fitted values and their 1σ confidence intervals for iron (Fig. 4A) are $z_0^{Fe} = 95 \pm 14$ Å and $2\sigma^{Fe} = 60\ ^{+20}_{-14}$ Å. The size of the ferritin core (8), measured by a scanning electron microscope (Hitachi S-900), agrees with the $2\sigma^{Fe}$ value obtained here. For BSA (Fig. 4B), $z_0^{Zn} = 63\ ^{+17}_{-31}$ Å and $2\sigma^{Zn} = 58\ ^{+26}_{-16}$ Å. The form of the BSA molecule, based on electron microscope observation with a metal coating (9), is a prolate ellipsoid with a major axis $2a = 140$ Å and a minor axis $2b = 40$ Å. Thus, our value of $2\sigma^{Zn}$ is in close agreement with the value of the short axis for the BSA molecules. Consequently, the experimental FXI pattern is consistent with a model in which the short axes of BSA molecules are perpendicular to the surface of the substrate.

Information obtained from our FXI fringes is similar to that from x-ray standing waves generated by total reflection (10). However, FXI measurements have some advantages (4). Parallel and monochromatic x-rays are unnecessary because fluorescent radiation occurs independently of the primary beam (11). Thus, white x-ray beams of synchrotron radiation, electrons, and ions can be used as the primary beam. We hope that the FXI method can effectively measure conformational changes for noncrystallized proteins in wet conditions.

REFERENCES AND NOTES

1. W. Kossel, V. Loeck, H. Voges, *Z. Phys.* **94**, 139 (1935).
2. M. v. Laue, *Ann. Phys. Leipzig* **23**, 705 (1935).
3. J. T. Hutton, G. T. Trammell, J. P. Hannon, *Phys. Rev. B* **31**, 6420 (1985).
4. Y. C. Sasaki, Y. Suzuki, Y. Tomioka, A. Fukuhara, *ibid.* **48**, 7724 (1993).
5. D. J. Hnatowich, W. W. Layne, R. L. Childs, *Int. J. Appl. Radiat. Isot.* **33**, 327 (1982).
6. Y. Tomioka, S. Imazeki, N. Tanaka, *Chem. Phys. Lett.* **174**, 433 (1990).
7. M. Born and E. Wolf, *Principles of Optics* (Pergamon, New York, 1980), chap. 1, pp. 55–70.
8. P. Fromherz, *Nature* **231**, 267 (1970).
9. A. Chatterjee and S. N. Chatterjee, *J. Mol. Biol.* **11**, 432 (1965).
10. M. J. Bedzyk, G. M. Bommarito, J. S. Schildkraut, *Phys. Rev. Lett.* **62**, 1376 (1989).
11. Y. Sasaki and K. Hirokawa, *Appl. Phys. A* **50**, 397 (1990).
12. A. F. S. A. Habeeb, *Anal. Biochem.* **14**, 328 (1966).

13. The authors thank Y. Tomioka for preparing the sample, A. Fukuhara for discussion, S. Imazeki for advice about charged LB film, and K. Kina for advice about labeling protein. This study was performed under the approval of the National Laboratory for High Energy Physics (proposal no. 93-Y003).

25 August 1993; accepted 29 October 1993

New Light on the Heart of Darkness of the Solar Chromosphere

S. K. Solanki,* W. Livingston, T. Ayres

Solar carbon monoxide spectra indicate the existence of a cool (less than 4000 kelvin) component to the solar chromosphere coexisting with the hot, bright gas at 6000 to 7000 kelvin. However, both the existence and the location of the cool component have been controversial. New high-resolution spectra show that carbon monoxide goes into emission just beyond the limb, allowing it to be probed without photospheric contamination. The cool component has temperatures as low as 3000 to 3500 kelvin and appears to cover 50 to 85 percent of the quiet solar surface. There is a steep temperature rise to normal chromospheric temperatures at a height of 900 to 1100 kilometers. Large horizontal velocities are seen, suggesting that the cool component is maintained by the supersonic adiabatic expansion of upwelling gas in overshooting granules.

The chromosphere of the sun is prototypical for the chromospheres of most cool stars. Any major challenge to the understanding of its structure will accordingly reverberate through many areas of solar and stellar physics. We report here on observations that strongly support the need for a fundamental revision of the traditional picture of the chromosphere as a relatively homogeneous thermal structure, with a temperature lying between 5000 and 7000 K over most of its height (1). Models based on this picture reproduce an impressive array of observations, mainly atomic spectral lines and continuous spectra, but possess one major flaw. They cannot match observations of the fundamental vibration-rotation band of the CO molecule at 4 to 5 μm (2). On the other hand, previous models based on the CO lines (2, 3) cannot be easily reconciled with the traditional optical and ultraviolet diagnostics. This inconsistency has led some researchers to doubt the very existence of a cold component (4, 5), and there is general agreement that its key properties—particularly the horizontal and vertical extents—are highly uncertain (6).

The major hindrance to the removal of these inconsistencies and uncertainties, the lack of high spatial resolution infrared instrumentation, has been overcome recently with the installation of a large infrared grating on the main spectrograph of the McMath-Pierce facility on Kitt Peak, near Tucson, Arizona. Spectra at 4.67 μm were obtained in April 1993 at the solar limb under conditions of exceptionally low smearing by the Earth's atmosphere and low atmospheric water vapor (Figs. 1 and 2). Outside the continuum limb the CO spectrum is clearly in emission.

From the observed continuum limb profile we first determined the spatial smearing due to the finite telescope aperture, spectrograph slit width, atmospheric blurring, and scattered light, assuming a regular limb. The observations were best reproduced without any atmospheric blurring. Perhaps a quiescent "random walk" atmosphere prevailed (7). We then used the inferred smearing and scattering parameters to estimate the true limb profile of the CO line core emission (Fig. 3). The brightness temperature of the optically thick CO line cores remains constant at 3600 to 3900 K to approximately 0.4 arc sec outside the 4.7-μm continuum limb (corresponding to the

S. K. Solanki, Institute of Astronomy, ETH-Zentrum, CH-8092 Zürich, Switzerland.
W. Livingston, National Solar Observatory, National Optical Astronomy Observatories, Tucson, AZ 85726.
T. Ayres, Center for Astrophysics and Space Astronomy, University of Colorado, Boulder, CO 80309–0391.

*To whom correspondence should be addressed.

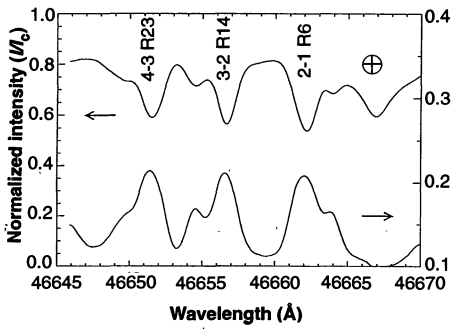

Fig. 1. Selected spectra observed near the north solar pole while the entrance slit was stepped across the solar limb at intervals of 0.3 arc sec. The upper spectrum lies inside the solar limb, exhibits absorption lines, and refers to the axis on the left. The lower spectrum lies outside the limb and refers to the right axis. The three main CO features are identified; the line marked with ⊕ is produced in the Earth's atmosphere. The off-limb spectrum exhibits emission features at the same wavelength as the CO absorption lines on the disk. The expression I/I_c denotes the intensity normalized to the continuum intensity at the center of the solar disk.

height of the traditional temperature minimum). Beyond that point the CO emission drops, albight less rapidly than the continuum. Although limb profiles that are less smooth than the ones shown in Fig. 3 are equally consistent with the data (the instrumental smearing is quite forgiving in this respect), our interpretations, like the data, are sensitive mainly to the following three gross features: the amplitude of the CO core emission at the spatial position of the continuum limb, I_0; the height at which the emission begins to drop, Z_0; and the "e-

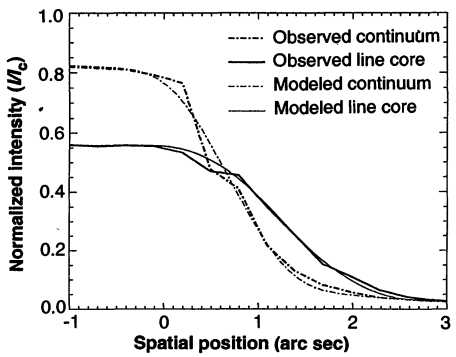

Fig. 2. Observed and synthesized profiles of the solar limb at a wavelength in the continuum and in the core of a CO transition. Negative spatial positions correspond to the solar disk. The origin of the spatial axis corresponds to optical depth unity at 5000 Å in the quiet sun at vertical incidence (the traditional origin of the height scale in solar atmospheric models). The line core intensity lies well below the continuum intensity on the solar disk (the signature of an absorption line) but above the continuum intensity beyond the limb (that is, an emission line).

folding" width, ΔZ, of the drop in emission beyond Z_0.

Next we calculated the CO limb profile in local thermodynamic equilibrium (LTE) (*8*), taking into account the solar curvature, for various hydrostatic atmospheric models. There are two main groups of models: those with a standard chromosphere [for example, the Vernazza-Avrett-Loeser–like models P and C (VALP and VALC), whose temperature stratification is plotted in Fig. 4 (*1*, *2*)], and those with a cold lower chromosphere (represented by 35COLD7 and 35COLD13 in Fig. 4). A grid of cold models for different heights of the steep temperature rise, Z_C, and minimum temperatures, T_C, was considered. The line core limb profiles for selected models are depicted in Fig. 3.

We were unable to devise a model based on a single thermal component that could reproduce the observations, despite trying a range of stratifications beyond those described above. Any single component failed to reproduce at least one of the main observational constraints described earlier. Greatly improved, although still not entirely satisfactory, fits were obtained with a two-component model: one hot (VALC or VALP-like), the second cool in the lower chromosphere ($T_C \approx$ 3000 to 3500 K), with a rise to higher temperatures at Z_C = 900 to 1100 km. The higher Z_C is only acceptable for $T_C \approx$ 3000 K, which corresponds roughly to the radiative equilibrium temperature in NLTE (*9*) and thus represents the lowest possible T_C (in a static atmosphere). The temperature of the hot component, T_H, the temperature of the cold component, T_C, and the filling factor of the hot component, α_H, are less well constrained than Z_C because they can partially compensate one another. For example, an increase in T_H can, within limits, be balanced by a decrease in α_H. There is, however, an independent constraint set by observed Ca II K line profiles, namely $T_{VALC} < T_H < T_{VALP}$ (*10*). With this relation we obtain 3600 K $\gtrsim T_C \gtrsim$ 3000 K.

A successful fit to the observations was obtained with a model possessing three components: (i) a hot component with filling factor α_H, (ii) a cold component with $Z_C \approx$ 900 km and filling factor α_{C1}, and (iii) a cold component with $Z_C \gtrsim$ 1000 km and filling factor $\alpha_{C2} = 1 - \alpha_H - \alpha_{C1}$. The model is specified by four main free parameters, T_H, T_C, α_H, and α_{C1}. Such a simulation is compared with the observed line-core and continuum limb profiles in Fig. 2. The parameters of this fit are $T_H \approx 0.8\ T_{VALP} + 0.2\ T_{VALC}$, $T_C \approx$ 3000 K, $\alpha_H \approx 0.40$, and $\alpha_{C1} \approx 0.35$. The best-fit parameter set is not unique, however, because there is a certain play-off between different parameters, as discussed for the two-component model.

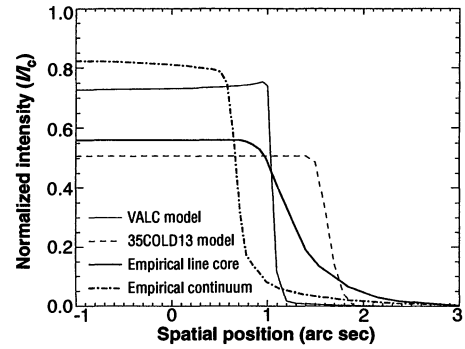

Fig. 3. Limb profiles in the continuum and in the core of the 3–2 R 14 transition. The thick curves have been derived empirically from the observations. The thin curves represent the limb profile in the core of the CO line resulting from single component models VALC and 35COLD13.

Nevertheless, our numerical experiments suggest that 25 to 50% of the solar surface is covered by a steep temperature rise at $Z_C \approx$ 900 km, while 25 to 35% is covered by such a rise at $Z_C >$ 1000 km. An upper limit on Z_C cannot be given because the limb profile of CO emission does not react significantly to large values of Z_C. We conjecture, however, that Z_C does not significantly exceed 1000 km over almost the whole solar surface, because at heights above approximately 1200 km most of the chromospheric volume apparently is hot according to far-ultraviolet emission of O I and C I (*5*).

The CO fundamental band lines belong to the few off-limb tracers of the chromospheric gas that can be satisfactorily reproduced by hydrostatic models (*11*, *12*). This relation supports the view that highly dynamic phenomena, such as spicules, which extend the chromospheric emission upward, are restricted to the hot (and probably magnetic) part of the chromosphere. Nevertheless, the CO lines support the presence of considerable dynamics in the cool component. The optically thin off-limb emission lines, which form purely in

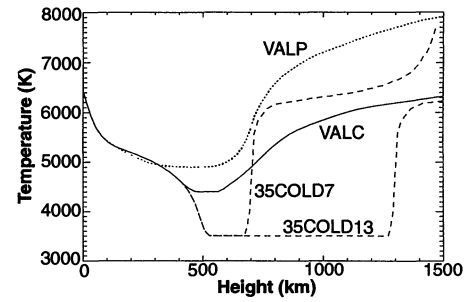

Fig. 4. Temperature versus geometrical height of four representative models. A geometrical height of 0 corresponds to spatial position 0 in Figs. 2 and 3.

the chromosphere, exhibit a significantly larger broadening than the absorption profiles on the disk (2 to 3 km s^{-1}) (*2*, *13*).

The large horizontal velocities implied by these excess line widths are reminiscent of the almost adiabatically expanding cool gas overlying granules in the upper reaches of granular simulations (*14*). Our observations suggest that on the real sun the convective overshoot does not stop at the temperature minimum, as is tacitly assumed in practically all current granular simulations, but continues into the lower chromosphere. In addition, the horizontal supersonic velocities seen in recent numerical simulations of solar convection (*15*, *16*) are possibly common in the dark heart of the lower chromosphere. One interpretation of the observations is that the CO lines form mainly in the granule centers, upstream of the shock fronts located near the downflow lanes. Hence, although the CO limb emission is well reproduced by hydrostatic atmospheres, the influence of convective dynamics on the stratification of the cool gas should be carefully investigated.

This cold chromospheric component survives even in the presence of substantial acoustic energy deposition (except at locations where the heating is particularly intense, such as magnetic elements) because of a combination of CO radiative cooling (*17*) and adiabatic expansive cooling. Energy deposition does produce a hot thermal zone overlying the cool layers (*4*, *18*). The magnetic field, which produces a magnetic canopy with a base close to Z_C (*19*), probably tends to stabilize the location of the steep rise of the temperature at the top of the heart of darkness of the solar chromosphere.

REFERENCES

1. J. M. Fontenla, E. H. Avrett, R. Loeser, *Astrophys. J.* **406**, 319 (1993).
2. T. R. Ayres, L. Testerman, J. W. Brault, *ibid.* **304**, 542 (1986).
3. T. R. Ayres and L. Testerman, *ibid.* **245**, 1124 (1981).
4. L. S. Anderson and R. G. Athay, *ibid.* **346**, 1010 (1989).
5. R. G. Athay and K. P. Dere, *ibid.* **358**, 710 (1990).
6. T. R. Ayres, in *Mechanisms of Chromospheric and Coronal Heating*, R. Ulmschneider *et al.*, Eds. (Springer, Heidelberg, 1991), p. 228.
7. M. Bester, W. C. Danchi, C. G. Degiacomi, L. J. Greenhill, C. H. Townes, *Astrophys. J.* **392**, 357 (1992).
8. T. R. Ayres and G. R. Wiedemann, *ibid.* **338**, 1033 (1989).
9. L. S. Anderson, *ibid.* **339**, 558 (1989).
10. S. K. Solanki, O. Steiner, H. Uitenbroek, *Astron. Astrophys.* **250**, 220 (1991).
11. L. M. Hermans and C. Lindsey, *Astrophys. J.* **310**, 907 (1986).
12. H. Zirin, *Astrophysics of the Sun* (Cambridge Univ. Press, Cambridge, 1988).
13. T. R. Ayres, *Astrophys. J.* **225**, 665 (1978).
14. R. Stein and Å. Nordlund, *ibid.* **342**, L95 (1989).
15. A. Malagoli, F. Cattaneo, N. H. Brumell, *ibid.* **361**, L33 (1990).
16. M. Steffen and B. Freytag, *Rev. Mod. Astron.* **4**, 43 (1991).
17. T. R. Ayres, *Astrophys. J.* **244**, 1064 (1981).
18. D. Muchmore, R. L. Kurucz, P. Ulmschneider, *Astron. Astrophys.* **201**, 138 (1988).
19. S. K. Solanki and O. Steiner, *ibid.* **234**, 519 (1990).

5 November 1993; accepted 24 November 1993

Void Structure in Colloidal Dispersions

Kensaku Ito, Hiroshi Yoshida,* Norio Ise†

The time evolution of void structures in highly purified polymer latex dispersions was studied with a confocal laser scanning microscope. In such dispersions, which were initially homogeneous, the voids grew with time when the dispersions were kept standing and formed more quickly in the internal material than in material close to the glass-dispersion interface. Void formation is thus not an artifact arising from the presence of the interface. A similar structural inhomogeneity, in apparently homogeneous systems, is discussed for simple ionic solutions, ionic polymer solutions, and Langmuir-Blodgett films.

Dilute polyelectrolyte solutions give a single, broad peak in the small-angle x-ray scattering profile which is attributed to the formation of an ordered structure (*1*). Although this interpretation of the peak was substantiated by a theoretical calculation of the scattering function by Matsuoka *et al.* (*2*, *3*), we were left with the intriguing result that the Bragg spacing between macroions in the ordered structure ($2D_{exp}$) (experimental uncertainty of order ±10%) was much smaller than the theoretical average spacing ($2D_0$) expected from the overall macroion concentration. For example, a fractionated sodium polyacrylate with 1470 monomer units had a $2D_{exp}$ value of 88 Å at a polymer concentration of 0.02 g/ml and 22°C, whereas the theoretical $2D_0$ was 222 Å. The same trend was observed for various ionic polymers, including highly charged globular proteins.

According to a simple stoichiometric consideration, the difference between the two spacings indicates that localized, non–space-filling ordered structures exist. The total sum of the volumes of these ordered structures must be 0.06 [$\approx(88/222)^3$] of the solution volume (although the volume of the single localized structure is not known), leaving 94% of the solution volume occupied by disordered macroions or voids. The coexistence of the ordered structure and free macroions appears to be supported by observation of slow and fast diffusion modes by dynamic light scattering (*4*).

Independently, Hachisu *et al.* (*5*) successfully observed under microscope void structures in dispersions of ionic polymer latex particles. This observation was confirmed by two groups (*6*–*8*), which reported huge and stable voids in apparently homogeneous dispersions. Voids were stable over about 10 hours and were observed even in samples several months old (*7*). Thus, we decided that the void structure must be considered if the true nature of interparticle interactions is to be sought. To eliminate the effect of the glass-dispersion interface (wall effect) in the void formation, we (*9*) used a confocal laser scanning microscope, which allowed observation of particles at a greater distance from the interface than previous microscopes (for example, even at 700 μm in a latex concentration of 0.01% for polystyrene-based particles in a D_2O-H_2O mixture). We found that huge, stable voids existed in the interior of the dispersion. Voids as large as 50 μm by 150 μm by 50 μm have been photographed (*10*).

The implication of the existence of such large and stable voids has recently been discussed (*10*). The voids testify to the presence of an attractive interaction between the colloidal particles. Here we describe a preliminary study of how the void structures in latex dispersions changed with time and depth from the top of the dispersion. The confocal laser scanning microscope (Carl Zeiss, Oberkochen, Germany) had a ×100 oil-immersion objective and a 5-mW Ar laser. We used styrene-based latex (N1000; diameter, 0.96 μm; charge density, 12.4 μC/cm^2; Sekisui Chemical, Osaka). The density was matched by selecting a D_2O-H_2O mixture. The dispersion temperature was kept constant with a thermostatted air bath. As described previously (*11*), latex dispersions were extensively washed with an Amicon Model 202 and a Diaflo XM300 with Milli-Q reagent-grade water. The dispersions were put into a container with highly purified ion exchange resins. The containers were allowed to stand or were rotated to facilitate rapid ion exchange until the resin particles started to

K. Ito, Department of Chemical and Biochemical Engineering, Toyama University, Toyama 930, Japan.
H. Yoshida, Department of Polymer Chemistry, Kyoto University, Kyoto 606-01, Japan.
N. Ise, Fukui Research Laboratory, Rengo Co., Ltd., Jiyūgaoko, Kanazu-cho, Sakai-gun, Fukui 919-06, Japan.

*Present address: Polymer Phasing Project, JRDC, Keihan-na Plaza, Seika-cho, Kyoto 619-02, Japan.
†To whom correspondence should be addressed.